

Inkjet Catalyst Printing and Electroless Ni-P Deposition for Fabrication of WWAN Antenna on PC/ABS Substrate

Yan-Yu Nian¹, Shu-Chuan Chen², Meng-Jey Youh³, Chang-Pin Chang^{3,*}, Zhi-Yu Luo³,
Ming-Der Ger^{3,*}

¹ School of Defense Science, Chung Cheng Institute of Technology, National Defense University, Taiwan 335, ROC

² Department of Electrical and Electronic Engineering, Chung Cheng Institute of Technology, National Defense University, Taiwan 335, ROC

³ Department of Information Technology, Hsing Wu University, Taiwan 244, ROC

⁴ Department of Chemical & Materials Engineering, Chung Cheng Institute of Technology, National Defense University, Taiwan 335, ROC

*E-mail: cpchang1@ndu.edu.tw (C.-P. Chang), mingderger@gmail.com (M.-D. Ger)

Received: 26 July 2016 / Accepted: 30 August 2016 / Published: 10 October 2016

In this study, a method to fabricate WWAN antenna on a PC/ABS alloy substrate is described. This method involves inkjet printing of a thermo-sensitive St-co-NIPAAm/Pd nanoparticle-based ink on PC/ABS substrate to create the catalytic site, onto which nickel is subsequently deposited by an electroless plating method, to obtain the desired metal pattern. Prior to electroless plating, pretreatments of PC/ABS by swelling and etching are utilized to improve the adhesion strength between PC/ABS substrate and electroless Ni-P coating. After the optimal swelling and etching treatments, the surface contact angle of PC/ABS decreases from 92° to 22° and the surface average roughness (Ra) increases from 329 to 2232 nm. The adhesion strength and corrosion resistance of the electroless Ni-P deposit increases as the pH value of the plating bath decreases. The maximum adhesion strength, about 2.3 MPa, is obtained at a bath pH of 5. Our result also demonstrates that this procedure is successfully applied for fabricating WWAN antenna with desired resonant frequencies.

Keywords: Inkjet printing; Electroless plating; Metal patterns; Antenna; PC/ABS

1. INTRODUCTION

PC/ABS is an alloy of polycarbonate and ABS, therefore, it offers the most desirable properties of both materials. With the rapid development of wireless communication systems, antenna embedded inside a tablet computer, personal computer, and cell phone are recently widely investigated. Thus, the metallization of PC/ABS has aroused great interest in recent years.

Concerning PC/ABS, the most popular metallization method reported in the literature is laser

direct structuring (LDS) [1-3]. LDS involves the use of special polymers (filled with organometallic complex or similar) and a laser structuring process, followed by electroless plating in the laser treated areas. This process, however, is expensive. Moreover, LDS is only suitable for relatively few commercial polymers [4, 5].

In recent times, a feasible process has been developed to generate high-resolution metal pattern on polymer substrate using inkjet printing and electroless plating techniques [6-10]. This method utilized inkjet printing of an ink on a polymer to create the catalytic site, onto which metal is subsequently deposited by an electroless plating method, to obtain the desired width and conductivity of the metal pattern. However, for the successful employment of metallized polymers into various applications, it is required to have good adhesion between a metal layer and a plastic substrate in order to prevent the peeling-off of deposited metal coatings during the usage period. Increasing surface roughness and changing surface functionality are generally utilized to improve the adhesion between the metal coating and polymer. Chemical etching with strong oxidizing agents is a common method to provide good adhesion between the metal coating and polymer substrate when acrylonitrile-butadiene-styrene (ABS) copolymer is used as the substrate. However, these oxidizing agents are generally toxic.

On the other hand, electroless metallization has to be preceded by an activity step that introduces the catalytic sites (palladium atoms and ions) onto the surface to be metallized. Generally, insulating substrates need to be sensitized and activated by dipping with a Sn/Pd as activator prior to use for electroless deposition [11]. However, the protective agent Sn^{2+} which prevented Pd from aggregating was easily oxidized to Sn^{4+} , leading to destroying the colloid stability and blocking nozzles. These limitations as well as environmental restrictions have created a continually growing demand for the development of new efficient and dependable processes.

In our previous works [12-14], a styrene-co-N-isopropylacrylamide (St-co-NIPAAm) oligomer with sulfate groups on chain end synthesized by free-radical copolymerization was used to reduce and disperse the Pd nanoparticles without any reducing agents or surfactant. Poly-N-isopropylacrylamide (PNIPAAm), an interesting thermo-responsive polymer, gained its popularity mainly because it has a fully reversible lower critical solution temperature (LCST) in water at around 305 K (32°C). When heated above 305 K, the polymer becomes hydrophobic and precipitates out from the aqueous solution; below the LCST it becomes completely soluble and forms a clear solution because of the transition into hydrophilic state [15]. According to the thermo-responsive characteristic of N-isopropylacrylamide, the St-co-NIPAAm/Pd nanoparticle showed good dispersion and excellent stability in the aqueous solution and can be used as an ink for microcontact printing and inkjet printing. When these printed Pd nanoparticles were further used as the activator for catalyzing electroless nickel, a nickel film with dramatically enhanced adhesion is formed on both PET and ITO glass surface without special pretreatment step. Utilization of this Pd ink as a precursor for electroless deposition appears to be a promising method for fabrication of metal patterns with high resolution.

In this study, the St-co-NIPAAm/Pd was further used as the activator for catalyzing electroless nickel (EN) on an etched PC/ABS substrate. Prior to electroless plating, the PC/ABS was etched by a mixture of hydroxyl peroxide and sulfuric acid to enhance the adhesion between the Ni coating and substrate. The effects of pH value of electroless plating bath and etching time on the characteristics of Ni coating was examined. In this paper we also demonstrated that it is indeed possible to fabricate

WWAN (wireless wide area network) antenna using the process combination of inkjet printing and electroless plating.

2. EXPERIMENTS

2.1 The preparation of thermal-responsive Pd nanocomposite

All chemicals in this work were of analytic grade purity and acquired from Merck. Styrene was purified at reduced pressure before use. All other chemicals were used as received. The thermal-responsive Pd ((St-co-NIPAAm)/Pd) nanocomposite was synthesized and characterized as described previously [16].

2.2 Pretreatment of substrate

The PC/ABS alloys with a brand name of TAIRILOY[®] AC3100 from FORMOSA CHEMICALS & FIBRE CORPORATION (Taiwan) were used as the substrates. Specimens were rinsed with acetone in an ultrasonic bath for 10 minutes, followed by washing with deionized water and drying in a cool air stream. Prior to inkjet printing, the sample was etched with a mixture consisting of four parts of H₂SO₄ and one part of 30% H₂O₂ at 100°C. The time of etching was controlled from 1 to 9 min in order to observe its influence on the hydrophilicity and surface roughness.

2.3 Electroless nickel plating

Prior to the actual electroless plating, the substrate was immersed in an activating solution at room temperature for 5 minutes to activate the surface. After rinsing in deionized (DI) water, the substrate was immersed into the EN plating solution (at 83°C) for the time specified in the text. The bath compositions which were used in the electroless plating process are presented in Table 1. The pH value of electrolyte was adjusted to 5, 7 and 9, respectively, to study its influence on the surface morphology, composition, deposition rate, and adhesion strength of the coating.

Table 1. Bath composition for the preparation of electroless Ni-P coating.

Composition	Content
NiSO ₄ · 6H ₂ O	19.5 g/L
NaH ₂ PO ₂ · H ₂ O	13 g/L
Sodium Lactate , NaC ₃ H ₅ O ₃	42 mL/L
Glycine , NH ₂ CH ₂ COOH , C ₂ H ₂ NO ₂	67 g/L
KIO ₃	20 ppm
PbNO ₃	1.5 ppm
H ₂ SO ₄ and NH ₄ OH	For adjusting of pH value

2.4 Fabrication of WWAN antenna

After pattern was designed, inkjet printing was performed using a commercially available piezoelectric Drop-on-Demand ink-jet Dimatix DMP 2800 printer (Dimatix-Rujifilm Inc., Santa Clara, USA). All samples were printed at room temperature. The activated substrate was first dried in a nitrogen atmosphere. The substrate was then immersed in an electroless Ni-P plating bath. The Ni-P coating was rinsed thoroughly with DI water and dried with nitrogen gas.

2.5 Characterizations

Scanning electron microscope (SEM, Jeol model JSM-6500) was employed to analyze the surface and cross-sectional morphology of the coatings with operating voltage of 15 kV. From cross-sectional micrographs of SEM, the thickness of the Ni-P film was estimated and the plating efficiency was calculated. There are five regions of each specimen selected randomly and be performed. The composition of the coatings was assessed with an electron probe X-ray micro-analyzer (EPMA, JEOL JXA-8200). The composition results were obtained from the average of 3 measurements. The average surface roughness (Ra) of the etched PC/ABS surfaces was measured using a surface roughness tester (KOSAKA- SURFCORDER SP81D). All roughness measurements were performed at a scan rate of 0.1mm/s over 12.50 mm length. The contact angle of the etched PC/ABS samples with water was measured by a contact angle goniometer (FACE CA-5 150, Tantec, USA) under room temperature. The contact angle and surface roughness of the as-received PC/ABS were also measured for comparison. The texture and grain size of the Ni-P coatings were determined using a X-ray diffractometer (XRD, Rigaku-RIMT 2000/PC). The electrical resistance was measured with a four-point probe (Napson RT-70).

The adhesion strength of the electrolessly deposited Ni-P with the substrates was determined by the pull-off adhesion test method described in the ASTM specification D 4541 [17] using an elcometer 106 adhesion strength tester. The metallized sample was adhered to an aluminum dolly using an adhesive. After the adhesive has cured, a tensile force is applied to the dolly axis. The force is gradually increased until the coating is detached. Thus the adhesion strength expressed in terms of the force is obtained. Thermal shock testing was performed followed MIL-STD-883E method [18] to determine the resistance to coating adhesion loss when subjected to sudden changes in temperature. Thermal shock tests were performed 5 cycles. Each cycle is consisted of 30 min holding in a temperature of 60°C, and then exposed to an extremely low temperature of -20°C for 30 min. The thermal shock resistance is determined by comparing the adhesion strength of the sample before and after thermal shock test.

Potentiodynamic polarization tests were carried out in a three-electrode cell system in which a platinum sheet and a saturated calomel electrode (SCE) were used as the counter and reference electrodes, respectively. The working electrode was a Ni-P coated sample. Geometric area of the tested specimens is 1 cm² in the corrosion experiments. The corrosion behavior of all samples was tested in a 3.5 wt.% NaCl aqueous solution at room temperature. All experiments were performed using an Autolab PGSTAT30 potentiostat/galvanostat controlled by the GPES (General Purpose

Electrochemical System) software. The linear polarization curves were measured in the potential range between -0.3 V and 0.8 V referred to open circuit potential, with a scanning rate of 0.5 mV s⁻¹. Before the tests, all specimens were rinsed with deionized water and stabilized at open circuit potential (OCP) for 30 min. A fresh corrosion bath was used for each new specimen.

The measurement of 3D far field radiation pattern was conducted in a far field antenna measurement system chamber (VSI-800F-10, Training research co., Taiwan). With this chamber, the return loss characteristic of the WWAN antenna was obtained. The frequency for which the return loss value is less than -6 dB is taken as resonant frequency of the antenna. The range of frequencies for which the return loss value is within the -6 dB points is usually treated as the bandwidth of the antenna.

3. RESULTS AND DISCUSSION

It is well known that ABS can be selectively etched by acid [19]. However, polycarbonates (PC) have tough surfaces owing to the existence of hydroxylatable functionalities on their structures, leading to PC cannot be sufficiently etched with common aqueous etchants. Pre-swollen PC is easy to degrade as the swelling provides a higher surface area and porous surface [20]. Therefore, a commercial phosphoric acid swelling agent (Fine-Will co., Taiwan) is used for pre-swelling PC/ABS. With the swelling treatment of an aqueous solution, some of PC phases in PC/ABS alloy were hydrolyzed, resulting in the change of surface contact angle. The effect of the swelling time on the surface contact angle was listed in Table 2. The original PC/ABS alloy was hydrophobic, and the surface contact angle between water and the substrate was 92° . It shows from Table 2 that the surface contact angle decreased initially with the swelling time and reached to a minimum value (62°) when the swelling time was 7 min. After the swelling treatment for 7 min, the PC/ABS substrate was etched with 1:4 H₂O₂:H₂SO₄ mix solution at 100°C for 1 to 9 min. The variation of surface contact angle with etching time is also displayed in Table 2. The surface contact angle showed a tendency to decrease with the etching time as the etching time increases from 1 to 5 min. A further increase of the etching time surpasses 5 min, a slightly increase in surface contact angle was observed. When compared with the swelling treatment results, the contact angle after etching treatment is lower than that before etching treatment. This result might be ascribed to that the PC/ABS surface changed from a hydrophobic to a hydrophilic due to the polar groups formed on the surface together with the creation of surface roughness after etching treatment. Thus, the wettability on the PC/ABS substrate surface was improved. This result is consistent with the literature report [21]. Then, the effect of the etching times on the surface morphology and surface roughness of the PC/ABS substrates were investigated, and the results are presented in Fig. 1 and Table 3, respectively. Fig. 1 displays the surface SEM images of PC/ABS substrates after etching for various times. Fig. 1(a) clearly demonstrates that the un-etched PC/ABS surface is smooth. However, in Figs. 1(b) to 1(f), the SEM micrographs of samples etched for 1, 3, 5, 7 and 9 min, respectively, illustrate a change in the surface morphology with voids and pores. With an increase of the etching time from 1 to 5 min, the density, size and depth of the cavities on the PC/ABS surface increases clearly, the roughness of the surface increases as the etching time increases. The surface roughness (Ra) of the PC/ABS substrate after etching for 5 min reaches the

maximum, 2232 nm. A further increase of the etching time to 7 or 9 min, an increase in the diameter of the cavities on the substrates surface and decrease in the depth of the cavities were observed, which can be attributable to the destruction of many bulk structures caused by longer etching time periods. By comparing Table 2 and Table 3, it is interesting to note that the etching time effects on surface contact angle and surface roughness are similar with each other, implying that the surface roughness of the substrate has direct relation with the wettability of the substrate. The minimum contact angle of about 62° was obtained after swelling for 7 min and etching for 5 min. Therefore, these pretreatment conditions were utilized for further study.

Table 2. Effects of swelling time and etching time on surface contact angle of PC/ABS.

Swelling time (min)	0	1	3	5	7	9
contact angle	92	85	72	65	62	63
Etching time (min) after swelling for 7 min	0	1	3	5	7	9
contact angle	62	57	40	22	27	36

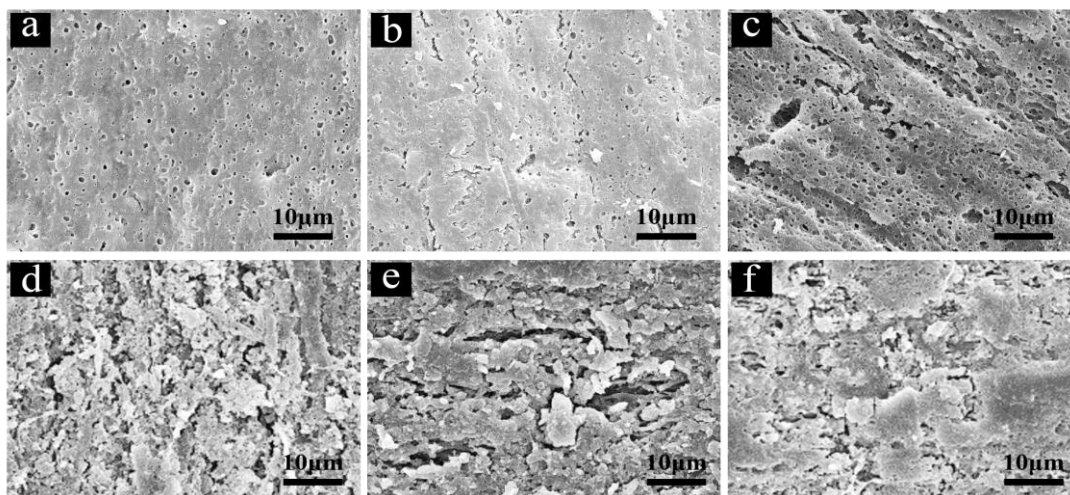


Figure 1. SEM images of PC/ABS substrates after etching with different times: (a) 0 min (b) 1 min (c) 3 min (d) 5 min (e) 7 min (f) 9 min.

Table 3. Effect of etching time on the surface roughness of PC/ABS.

Time	0	1	3	5	7	9
Surface average roughness Ra(nm)	329	847	1147	2232	1507	1235

In order to investigate the pH effect on the crystallinity and deposition rate of the electroless Ni–P deposits, the various bath pH values (pH 5, 7, and 9) and the various deposition times (10, 20, and 40 min) were used. The SEM surface images of the Ni–P layers deposited under different

conditions are shown in Fig. 2a-i, respectively. It can be seen from Fig. 2 that the variation in surface morphology of these coatings suggests a definite dependence on their bath pH values and deposition times. It can be seen from Fig. 2a, 2b and Fig. 2c that the grain size of Ni-P deposits grows with plating time. By comparing Fig. 2a, 2d and Fig. 2g, it shows that the grain size increases with the pH value of the plating bath. This result suggests that the pH value of the plating bath will affect the deposition rate. The higher the pH is, the higher is the deposition rate. Fig. 3 shows the cross-sectional SEM images of the Ni coating plated at various pH values for 40 min. As shown from this figure, the thickness of the coating is 6.04 μm , 9.60 μm and 10.79 μm , respectively, for plating at pH=5, pH=7 and pH=9, which is consistent with the finding as shown in Fig. 2. This result is expectable. It is well known that the pH of the plating bath will affect both reduction reactions of nickel and phosphorus ions. Increasing the pH facilitates the nickel-reduction reaction while is harmful to the phosphorus reduction.

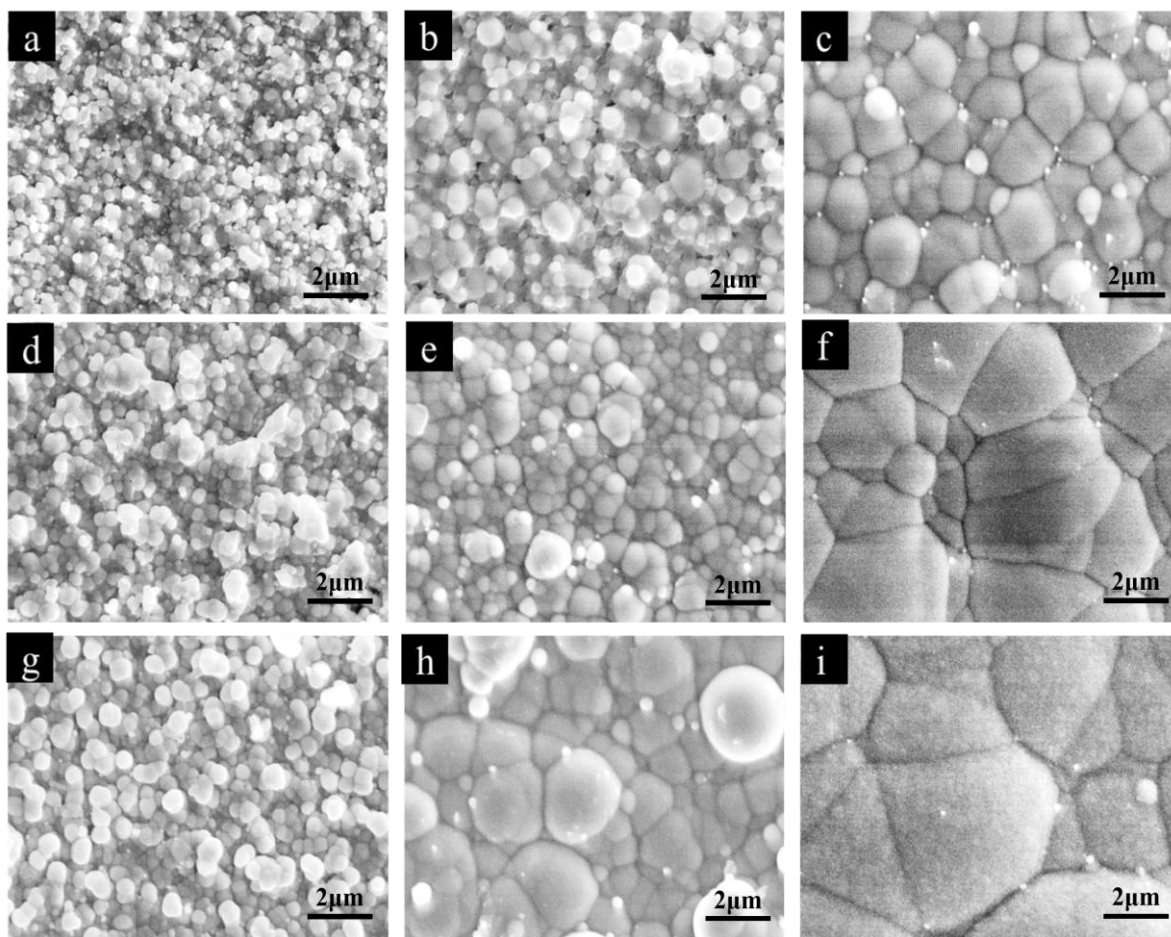


Figure 2. The SEM surface images of Ni-P coatings deposited at 83°C for 10 min at pH 5 (a), 20 min at pH 5 (b), 40 min at pH 5 (c), 10 min at pH 7 (d), 20 min at pH 7 (e), 40 min at pH 7 (f), 10 min at pH 9 (g), 20 min at pH 9 (h), and 40 min at pH 9 (i).

Therefore, increasing the pH of the solution decreases the phosphorus content of the coating. Also, since the nickel reduction reaction predominantly controls the deposition rate, increasing the pH of the solution increases the deposition rate. As the pH of plating bath increasing, the phosphorous

content of Ni-P coatings is decreasing. It is well known that the crystallization behavior of nickel-phosphorous deposits depends on the level of phosphorous content. Thus, the pH of nickel plating solutions effect on Ni-P coatings structure was studied. Fig. 4 displays the XRD pattern of Ni-P coatings deposited on the substrate from bath solutions having different pH values. From Fig. 4, results show that the pH of nickel plating solutions had a significant effect on the crystalline behavior of Ni-P coating. The higher pH conditions tend to produced higher crystalline structure of Ni-P coatings than lower pH plating bath. For pH 5, the Ni-P coating shows a low and broad peak intensity near 44 degree which indicates that amorphous type of Ni-P coating was produced during plating. Table 4 lists the electrical properties of the Ni-P coatings.

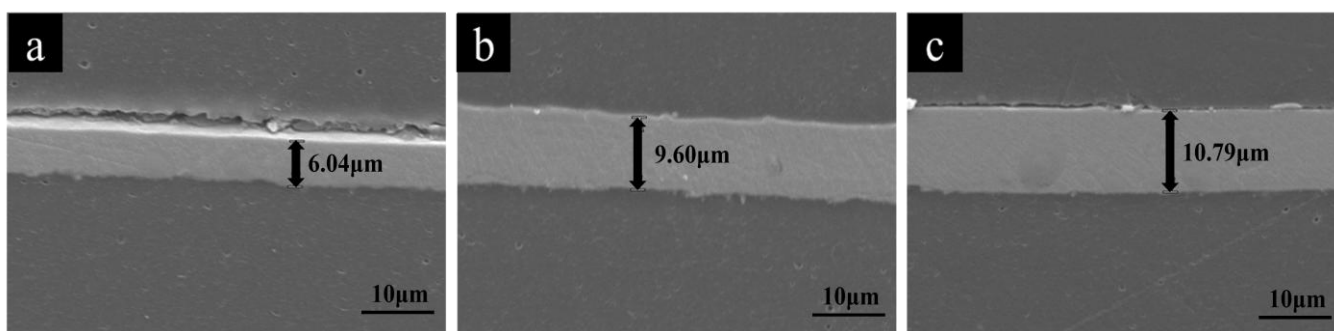


Figure 3. The SEM cross-sectional images of the Ni-P coatings deposited for 40 min at pH of 5 (a), pH of 7 (b), and pH of 9 (c).

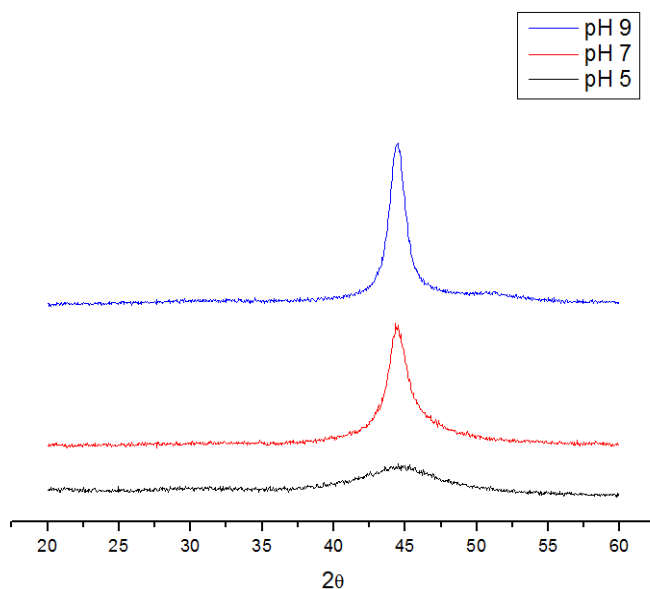


Figure 4. XRD pattern of Ni-P coatings deposited on the PC/ABS substrate from bath solutions having a pH value of 5, 7 and 9, respectively.

The resistivity of pure nickel is $7.8 \times 10^{-6} \Omega\text{-cm}$. However, the resistivities of electroless nickel phosphorus coating are higher than that of pure nickel due to the co-deposition of phosphorus inside electroless nickel deposits. With a low phosphorous content, the sheet resistance and the resistivity of

Ni-P coating deposited from bath with a pH of 9 is $0.12 \text{ } \Omega/\text{sq}$ and $1.29 \times 10^{-6} \text{ } \Omega\text{m}$, respectively. However, the sheet resistance of $0.34 \text{ } \Omega/\text{sq}$ and the resistivity of $2.05 \times 10^{-6} \text{ } \Omega\text{m}$ were found for Ni-P coating deposited from bath with a pH of 5. Thus, the resistivity increases with increasing phosphorus content. Although the resistivity of Ni-P coatings prepared in the present study is about ten times higher than that of pure nickel, it is superior to those reported in literatures for nanoparticles containing inks [22-24].

Table 4. The thickness and electrical properties of Ni-P coatings deposited at various bath pH values.

	pH=5	pH=7	pH=9
Thickness (μm)	6.04	9.60	10.79
Sheet resistance (Ω/sq)	0.34	0.15	0.12
Electrical resistivity (Ωm)	2.05×10^{-6}	1.44×10^{-6}	1.29×10^{-6}

The adhesion properties of coatings on antennas are important characteristics affecting the performance of antennas. In order to study the adhesion properties of EN coatings a pull-off adhesion test method using an elcometer 106 adhesion strength tester was conducted. The pull-off test is schematically depicted in Fig. 5 and the measured adhesion strengths for Ni-P coatings deposited at various bath pH values are presented in Table 5. From Table 5, it can be clearly seen that the greatest adhesion strength was found in the coating obtained at pH 5 and the adhesion strength decreased with increasing bath pH. This might be ascribed to the fact that the thicker coating with less phosphorus content was formed at high bath pH value. The thicker coatings with less phosphorus content are more brittle and consequently more prone to cracking, resulting in a lowering of adhesion strength. On the other hand, the effect of thermal shock testing on the adhesion properties of EN coatings is more pronounced in high-phosphorus EN coatings. After thermal shock testing, the adhesion strength of Ni-P coating deposited at pH 5 shows 25% decrease from 2.30 MPa to 1.73 MPa, whereas the adhesion strength reduction for Ni-P coating deposited at pH 7 and 9 after thermal shock testing is only 15 % and 14 %. This might be attributed to the difference in thermal expansion coefficient between high-phosphorus EN coating and low-phosphorus EN coating. Generally, the thermal expansion coefficient of EN coatings is between 10×10^{-6} and $25 \times 10^{-6} \text{ m/m K}$ [25], and the thermal expansion coefficient decreases with increasing phosphorus content. On the other hand, the thermal expansion coefficient of PC/ABS alloys is in the range from $70 \times 10^{-6} \text{ m/m K}$ to $73 \times 10^{-6} \text{ m/m K}$ [26]. The mismatch of Coefficient of thermal expansion (CTE) is one of the factors that may affect the interfacial residual stress and the bond strength. If the CTE mismatch between the coating and the substrate is high enough, the tensile stresses caused by the mismatch of Coefficient of thermal expansion may lead to crack growth and spontaneous failure. Therefore, the detrimental effect of thermal shock testing on adhesion strength is more pronounced for high phosphorus EN coating compared with that of low phosphorus EN coatings.

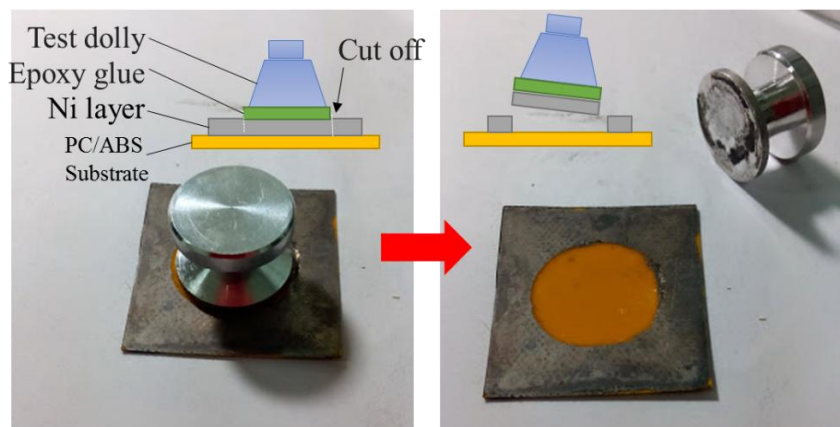


Figure 5. Schematic illustration of pull-off adhesion test.

Table 5. The adhesion strength between Ni-P coatings and PC/ABS alloy before and after thermal shock testing.

Bath pH value	5	7	9
The adhesion strength of coating (MPa)	2.30	1.85	0.92
The adhesion strength of coating after thermal shock testing (MPa)	1.73	1.57	0.79

The polarization curves obtained for Ni-P coatings deposited at various bath pH values, in 3.5% sodium chloride solution, are shown in Fig. 6. The corrosion parameters, including corrosion potential (E_{corr}), corrosion current density (I_{corr}), anodic Tafel slope β_a and cathodic Tafel slope β_c , derived from polarization curves are presented in Table 6. The corrosion potential and corrosion current density are calculated using Tafel extrapolation method. The corrosion current densities of the Ni-P coatings deposited at bath pH of 5, 7 and 9 are $9.96 \times 10^{-6} \text{ A/cm}^2$, $9.72 \times 10^{-6} \text{ A/cm}^2$ and $5.9 \times 10^{-5} \text{ A/cm}^2$, respectively. On the other hand, the corrosion potentials of the Ni-P coatings deposited at bath pH of 5, 7 and 9 are -0.058 V, -0.095V and -0.235 V, respectively. In a typical polarization curve, more positive corrosion potential and lower corrosion current density correspond to lower corrosion rate and better corrosion resistance of the coating. Apparently, the corrosion resistance of the amorphous Ni-P coating deposited at pH 5 is superior to those crystalline coatings deposited at a higher pH value. As mentioned above, the coating thickness increases with the increasing of bath pH value. It is interesting to note that the much thicker Ni-P coating formed at pH of 7 and 9 show less protection than the coating formed at pH of 5. The superior corrosion protection provided by Ni-P coating deposited at pH of 5 can be attributed to this coating is amorphous. The higher corrosion resistance of amorphous electroless Ni-P coatings is due to their homogeneous structure and the absence of grain boundaries [27], which will decrease the passages for the eroding Cl^- anions entering into the coating. A similar result for the phosphorus content effect on corrosion resistance of Ni-P coating had been reported by Lu et al. [28].

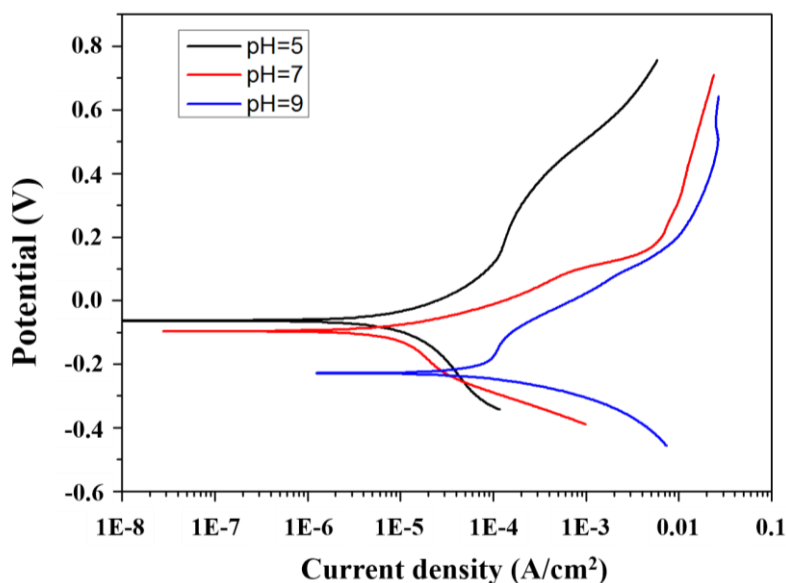


Figure 6. Potentiodynamic polarization curves of the electroless Ni-P coatings deposited at various bath pH values in 3.0 wt% NaCl solution.

Table 6. Corrosion characteristics of Ni-P coatings deposited at various bath pH values

Coatings	β_a (V/decade)	β_c (V/decade)	E_{corr} (V)	I_{corr} ($\mu A/cm^2$)
pH=5	0.143	0.196	-0.058	9.96
pH=7	0.139	0.194	-0.0953	9.72
pH=9	0.167	0.129	-0.235	59

Although the Ni-P coating deposited at bath pH of 5 is inferior to Ni-P coating deposited at a higher bath pH value in electrical conductivity, it was selected for preparation of WWAN antenna. The reason for that is the Ni-P coating deposited at bath pH of 5 has the highest adhesion strength and corrosion resistance among all tested samples. After pretreatments by swelling and etching with the optimal conditions as described in above, the St-NIPAAAM ink was inkjet printed on the PC/ABS substrate, followed by electroless Ni-P plating at bath pH of 5 for 40 min. The thickness of Ni-P coating is about 6 μm . Fig. 7 displays the optical image of the fabricated WWAN antenna. Fig. 8 shows the measured return loss of the fabricated antenna shown in Fig. 7. Note that in the desired operating bands, the impedance matching is better than -6 dB return loss (3:1 VSWR), which is the widely used design specification for the internal WWAN handset antennas [29-33]. It shows from Fig. 8 that the resonant frequency of the antenna obtained in present study covers the desired 824–960 and 1710–2170 MHz bands for the WWAN operation. This study demonstrates that the integration of inkjetting with electroless plating onto PC/ABS can be used to fabricate the WWAN antenna. °

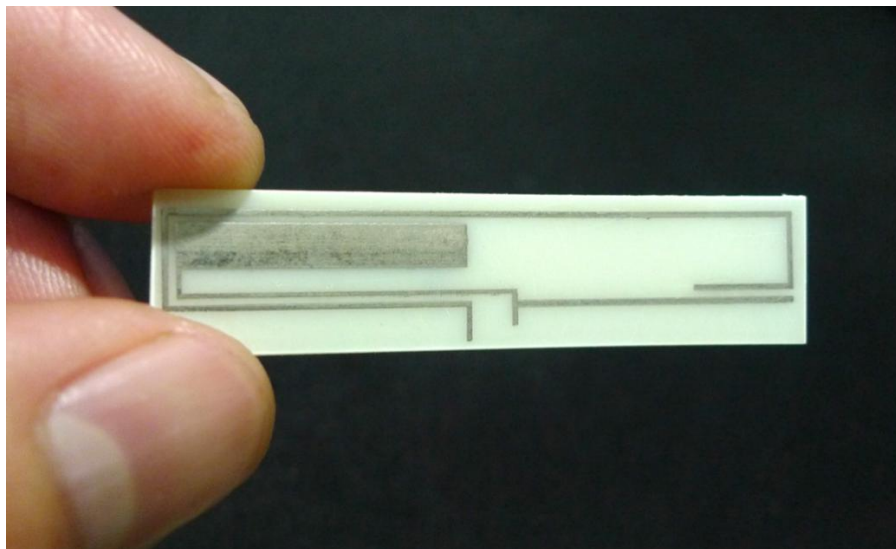


Figure 7. Photo of the fabricated WWAN antenna.

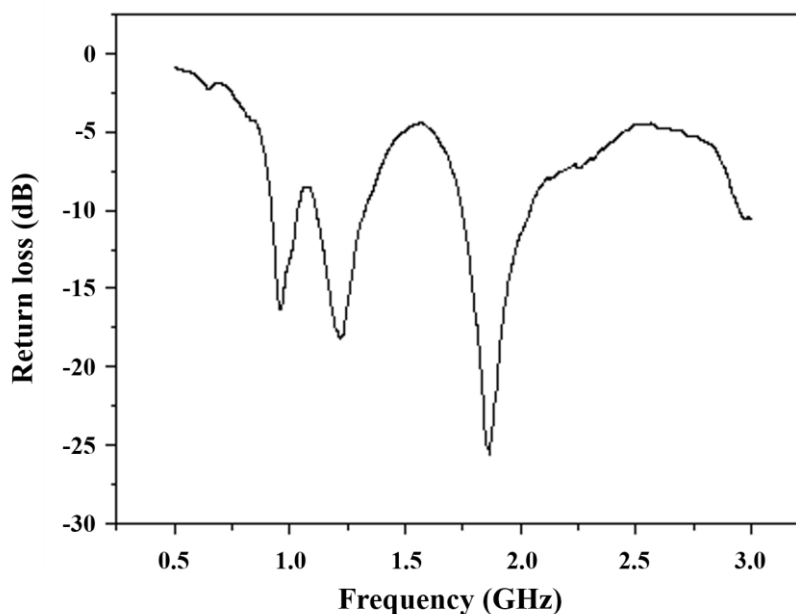


Figure 8. Measured return loss for the WWAN antenna against the operating frequency.

4. CONCLUSION

1. When the PC/ABS substrates were treated in optimal swelling and etching conditions, a preferable surface topography with surface roughness ($R_a=2232$ nm) were achieved. Many cavities appeared on the surface were observed, which facilitate the Ni-P metallization onto the PC/ABS substrates.

2. The characteristics of electroless Ni-P coatings were dependent on the bath pH value. Lower pH of plating bath produced low crystallinity structure of Ni-P coatings compare to higher pH of plating bath. And the maximum adhesion strength between PC/ABS surface and electroless Ni-P

film deposited at bath pH of 5 reached to 2.3 MPa..

3. The sheet resistance and the resistivity of Ni-P coating deposited from bath with a pH of 9 is 0.12 Ω /sq and 1.29×10^{-6} Ω m, respectively, whereas the sheet resistance of 0.34 Ω /sq and the resistivity of 2.05×10^{-6} Ω m were found for Ni-P coating deposited from bath with a pH of 5. Although the resistivity of Ni-P coatings prepared in the present study is about ten times higher than that of pure nickel,

4. Substrate with optimal surface pretreatments were identified, and WWAN antenna was fabricated on it using a combination of inkjet printing and electroless plating.

ACKNOWLEDGEMENTS

This study is sponsored by National Science Council of Taiwan under Grant No. MOST 105-2623-E-606-003-D.

References

1. G. Naundorf and H. Wissbrock, Conductor track structures and method for production thereof, US Patent Application US7060421 B2
2. G. Naundorf, Method for the production of a printed circuit structure as well as a printed circuit structure thus produced, US Patent Application US20070247822 A1
3. G. Naundorf, Method for production of a conductor track structure and a correspondingly produced conductor track structure, WIPO Patent Application WO2007115546 A2
4. M. Hüske, J. Kickelhain, J. Müller and G. Eber, *Laser Supported Activation and Additive Metallization of Thermoplastics for 3D-MIDs*, Proc. 3rd LANE 2001, Germany, 2001
5. G. Naundorf and H. Wißbrock, *Metalloberfläche* 11(2000) 29
6. B. S. Cook, Y. Fang, S. Kim, T. Le, W. B. Goodwin, K. H. Sandhage and M. M. Tentzeris, *Electron. Mater. Lett.* 9(2013) 669
7. A. Sridhar, J. Reiding, H. Adelaar, F. Achterhoek, D. J. Van Dijk and R. Akkerman, *J. Micromech. Microeng.* 19(2009) 085020.
8. S. Ma, L. Liu, V. Bromberg and T. J. Singler, *ACS appl. Mat. interfaces* 6 (2014) 19494
9. Y. Chang, C. Yang, X. Y. Zheng, D. Y. Wang and Z. G. Yang, *ACS appl. Mat. interfaces* 6 (2014) 768
10. P. C. Wang, C. P. Chang, M. J. Youh, Y. M. Liu, C. M. Chu and M. D. Ger, *J. Taiwan Inst. Chem. Eng.* 60(2016) 555
11. R. L. Cohen, K. W. West, *Chem. Phys. Lett.* 16(1979) 128
12. W. D. Chen, C. P. Chang, Y. Sung, Y. M. Liu and M. D. Ger, *Surf. Coat. Tech.* 205 (2011) 4750
13. Y. M. Liu, N. W. Pu, W. D. Chen, K. H. Lin, Y. Sung, M. D. Ger, C. L. Chang and T. L. Tseng, *Microelectron. Reliab.* 52 (2012) 398
14. C. P. Chang, P. C. Wang, Y. Y. Nian, Y. M. Liu and M. D. Ger, *J. Taiwan Inst. Chem. Eng.* 45 (2014) 2755
15. S. Ito, *Kobunshi Ronbunshu* 46 (1989) 437.
16. W. D. Chen, Y. Sung, C. P. Chang, Y. C. Chen, M. D. Ger, *Surf. Coat. Tech.* 204 (2010) 2130
17. ASTM D4541, Standard Test Method for Pull-Off Strength of Coatings Using Portable Adhesion Testers, ASTM International. West Conshohocken, Pennsylvania, United States (2009)
18. Department of Defense USA, MIL-STD-883E, Test Method Standard, Micro-circuits, Method 1011.9 (1995)
19. S. Olivera, H. B. Muralidhara, K. Venkatesh, K. Gopalakrishna and C. S. Vivek, *J. Mater. Sci.* 51

(2016) 3657

20. G. N. Patel, D. Bolikal, R. A. Bellemare, Pre-swelling and etching plastics for plating, US patent 5,015,329 (1991).
21. Q. Ma, W. Zhao, X. Li, L. Li, Z. Wang, *International Journal of Adhesion & Adhesives* 44 (2013) 243
22. Q. Huang, W. Shen, Q. Xu, R. Tan and W. Song, *Mater. Lett.* 123 (2014) 124
23. J. Niittynen, R. Abbel, M. Mäntysalo, J. Perelaer, U. S. Schubert and D. Lupo, *Thin Solid Films* 556 (2014) 452
24. M. Makrygianni, I. Kalpyris, C. Boutopoulos¹, I. Zergioti, *Appl. Surf. Sci.* 297 (2014) 40
25. Q. Huang, W. Shen, Q. Xu, R. Tan, W. Song, *Mater. Chem. Phys.* 147 (2014) 550
26. Z. K. Kao, S. P. Chen, J. L. Lin, Y. C. Liao, *J. Taiwan Inst. Chem. Eng.* 43 (2012) 965
27. T.S.N. Sankara Narayanan, I. Baskaran, K. Krishnaveni, S. Parthiban, *Surf. Coat. Tech.* 200 (2006) 3438
28. G. Lu and G. Zangari, *Electrochim. Acta.* 47 (2002) 2969-2979.
29. F. H. Chu and K. L. Wong, *IEEE Trans. Antennas Propag.* 58 (2010) 3426
30. K. L. Wong, W. J. Chen, L. C. Chou, and M. R. Hsu, *IEEE Trans. Antennas Propag.* 58 (2010) 3431
31. Y. L. Ban, S. C. Sun, J. L. W. Li, and W. Hu, *J. Electromagn. Waves & Appl.* 26 (2012) 2222
32. K. L. Wong, Y. W. Chang and S. C. Chen, *IEEE Trans. Antennas Propag.* 60 (2012) 1705
33. Y. L. Ban, J. H. Chen, J. L. W. Li, and W. Hu, *J. Electromagn. Waves & Appl.* 26 (2012) 2211

© 2016 The Authors. Published by ESG (www.electrochemsci.org). This article is an open access article distributed under the terms and conditions of the Creative Commons Attribution license (<http://creativecommons.org/licenses/by/4.0/>).